Available online at www.eccomasproceedia.org
Eccomas Proceedia COMPDYN (2017) 1558-1573

ECCOMAS
Proceedia

COMPDYN 2017
6th ECCOMAS Thematic Conference on
Computational Methods in Structural Dynamics and Earthquake Engineering
M. Papadrakakis, M. Fragiadakis (eds.)
Rhodes Island, Greece, 15–17 June 2017

RINTC PROJECT: NONLINEAR DYNAMIC ANALYSES OF ITALIAN CODE-CONFORMING STEEL SINGLE-STOREY BUILDINGS FOR COLLAPSE RISK ASSESSMENT

Fabrizio Scozzese[1], Giusy Terracciano[2], Alessandro Zona[1], Gaetano Della Corte[2], Andrea Dall'Asta[1], Raffaele Landolfo[2]

[1] University of Camerino
School of Architecture and Design, Viale della Rimembranza, 63100 Ascoli Piceno, Italy
e-mail: fabrizio.scozzese@unicam.it, alessandro.zona@unicam.it, andrea.dallasta@unicam.it

[2] University of Naples Federico II
Dept. of Structures for Engineering and Architecture, via Claudio, 21 Naples, Italy
e-mail: giusy.terracciano@unina.it, gdellaco@unina.it, landolfo@unina.it

Keywords: steel structures, nonlinear static and dynamic analyses, concentric brace models, steel fracture criteria, multi-stripe analyses, risk assessment.

Abstract. *This paper reports on the results of an ongoing Research Project aimed at computing the risk of collapse in new buildings conforming to the Italian Seismic Design Code. Companion papers describe the overall Research Project, funded by the Italian Civil Protection Department (DPC), its different areas of application (reinforced concrete, masonry, steel buildings, etc.), the overall seismic risk calculation procedure and the ground motion selection process followed to identify the recorded ground motions used for the multi-stripe analyses for twenty different ground motion intensities. Specifically, steel structures are considered within this paper and the nonlinear modelling and analysis of steel single-storey buildings designed in cities with increasing seismic hazard are described. First, the paper presents the geometry, material characteristics and main design properties of the buildings, including their elastic dynamic properties. Second, the paper introduces the nonlinear models used for the nonlinear analyses: distributed plasticity models for beams, columns, and concentric braces including geometric imperfections for triggering of buckling. Pushover analyses are used for a preliminary evaluation of the nonlinear behaviour under increasing horizontal loads. Afterwards, the main results of the multi-stripe dynamic analyses are presented for different ground motion intensities.*

Peer-review under responsibility of the organizing committee of COMPDYN 2017.
doi: 10.7712/120117.5513.17301

1 INTRODUCTION

In this paper, the seismic behaviour of non-residential single-storey steel buildings is investigated through the use of a material and geometric nonlinear finite element model. The goal is the development of a numerical tool able to describe the structural performance of such structural system up to collapse under increasing seismic intensities, in line with the goal of the project [1], i.e. the implicit risk associated with the current Italian code [2] when designing new structures in different site locations corresponding to three levels of seismic hazard. Details on the project goals and methodologies are available in the companion papers.

2 CASE STUDY STRUCTURES

2.1 Description of the structural system

The considered structural system is composed of five single span duo-pitch portal frames repeated in the longitudinal direction with a constant spacing. The frames are connected in the longitudinal direction by hot-rolled beams at the apex, at the eaves and at the crane-supporting bracket level (Figure 1). Gravity loads are supported by all members while horizontal forces are withstood by two different seismic-resistant structure typologies acting along two orthogonal directions. In the X-direction the resistance to lateral forces is mainly due to continuous and rigid frame action. In the Y-direction the resistance to horizontal forces is provided by vertical bracings placed in the outer spans of the building. Secondary structural elements are also considered. Purlins, used to support the roof cladding and positioned every 2.5 m, transfer the forces from the roof cladding to the rafters. Roof bracings are arranged in the outer bays to transfer horizontal forces to the vertical bracings.

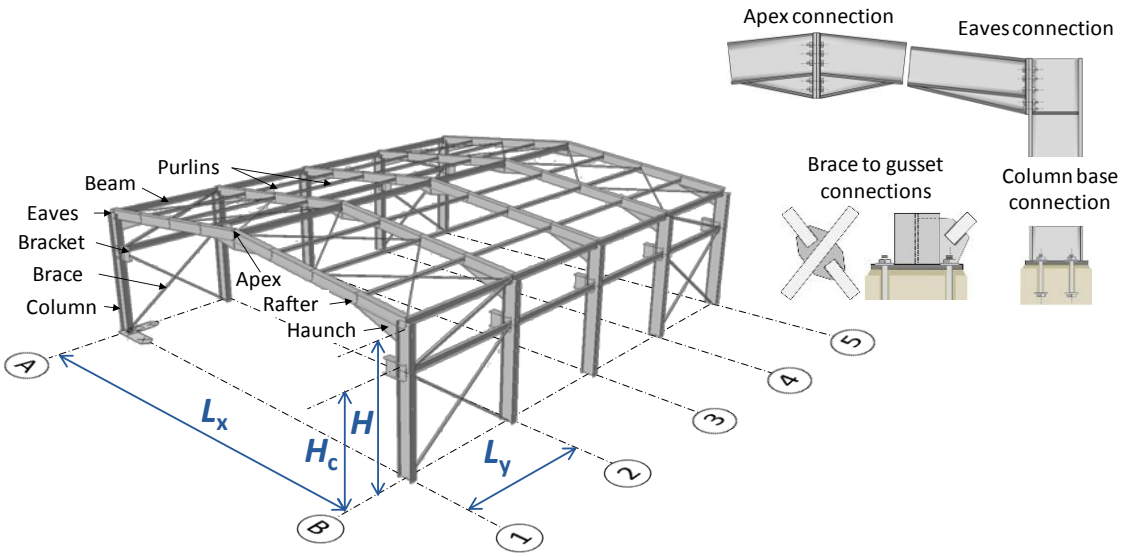

Figure 1: Description of the structural system.

The structural efficiency of portal frames is based on the use of moment resisting connections between beams and columns. The case study structures assumed the adoption of full-strength bolted end-plate connections at eaves and apex. As typical for this structural type, the rafter connection to the column comprises a haunch used to improve the performance of the rafter and facilitate a bolted connection to the column. In this study, the length of the eaves' haunch is assumed as equal to 10% of the span. To facilitate the bolted connection, small

haunches are considered at the apex too. The roof purlins are connected to the rafters by pinned connections and assumed as simple spanned between two consecutive frames. All the columns are assumed as hinged at their base. Hot-rolled I or H sections are used for beams, columns and purlins. Cold-formed steel square hollow sections are chosen for vertical braces, while hot-rolled L-shaped profiles are used for roof bracings. The selected steel grade is S275 (characteristic value of the yield strength f_{yk} = 275 N/mm^2, the characteristic tensile strength of the material f_{tk} = 430 N/mm^2 and the Young Modulus E = 210000 N/mm^2).

2.2 Design configurations

The transverse bay width (L_x), the longitudinal bay width (L_y), the height at the eaves (H) and the height of the crane-supporting bracket (measured at top surface of the bracket) are assumed as design parameters (Figure 1). Four geometrical configurations are selected, as shown by the parameter values provided in Table 1. In all cases, the roof pitch is equal to 6°.

Structural system	L_x, H, H_c, (m, m, m)	L_y (m)
1	20, 6, 4.5	6.00
2	20, 6, 4.5	8.00
3	30, 9, 6	6.00
4	30, 9, 6	8.00

Table 1: Geometry parameters for the considered case studies.

To characterize variable loads and seismic actions, the considered structural systems are assumed located in three different Italian sites: L'Aquila, Naples and Milan. For the seismic input two soil types were considered: type A and type C. Combining the geometrical properties with the features of location sites, twenty-four design configurations are derived (Figure 2). Each design configuration is labelled with an alphanumerical string containing the main geometrical parameters characterizing the case study, in the following order: transverse bay width (Lx20 or Lx30), longitudinal bay length (Ly6 or Ly8), site location (AQ, NA, MI) and soil type (A or C).

2.3 Linear finite element models for the design

The global behaviour of the case study structures are analysed by the structural analysis program MIDAS Gen ([3]). A 3D model is adopted and both the beams and the columns are represented by two nodes beam elements, taking into account the stiffness effects of tension/compression, shear, bending and torsional deformations. Two-node truss elements are used to model longitudinal and roof braces, representing uniaxial tension-only members. Pinned end connections are introduced by the Beam End Release option available in Midas. Column base connections are represented by pinned restraints.

Horizontal forces are mainly resisted by the continuity of the frame structure in the transverse direction (X) and by members subjected to axial forces in the longitudinal direction (Y). Following the current European [4] and Italian seismic code [1], the design model assumed that horizontal forces can be resisted by tension-only diagonal braces, i.e. the contribution of the compression diagonals to the lateral force resistance is neglected at the design stage.

A travelling overhead crane is considered and its runway beams are assumed to be the same for all cases and made of a HEA400 steel beam. The crane runway beam is explicitly

included in the global analysis model and its presence taken into account by equivalent static actions on the column brackets.

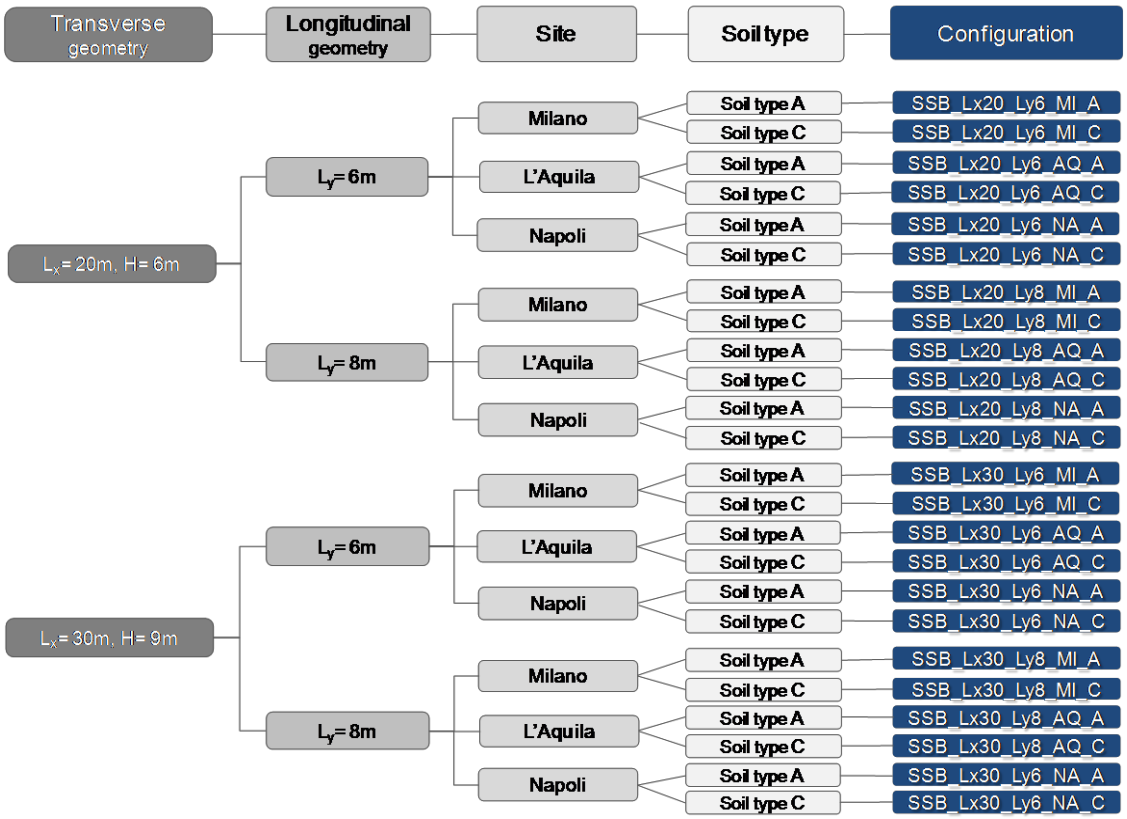

Figure 2: Design configurations.

2.4 Actions and design load combinations

Self-weights of structural elements are directly accounted by the software. Self-weight of non-structural elements, such as the roof and wall claddings, are also classified as permanent loads. Claddings used in this study are represented by profiled composite panels for roofs and flat panels for side walls. Their loads are modelled as uniformly distributed loads on the roof purlins (G_{roof}) and columns (G_{wall}). The travelling crane self-weight (G_c), as well as the weight of the runway beams ($G_{b,c}$), are modelled as concentrated forces acting on the top of the column bracket which is supposed to be welded to the column flange (Figure 3).

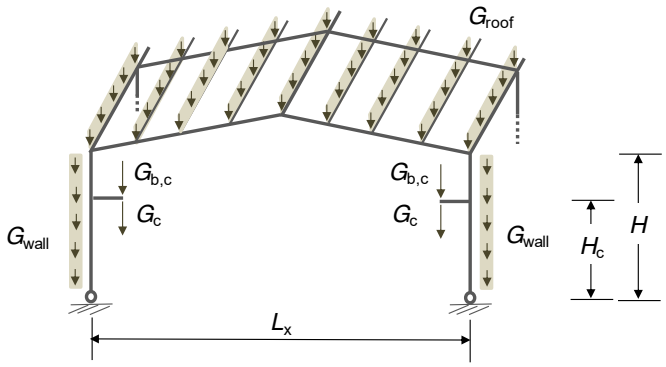

Figure 3: Permanent loads modelling.

Wind actions are represented by a set of pressures both normal and parallel to structure's surfaces. The magnitude of normal pressures is calculated by the NTC 2008 [2] formulas based on the parameters in Table 2 (i.e., the wind zone, the altitude of the site from the sea level a_s, the wind velocity v_b, the basic velocity pressure q_b, the exposure coefficient c_e, the the dynamic coefficient c_d). The external pressure coefficients $c_{p,}$ are assumed, according to the Italian code, depending on the wind direction and the slope of the walls. Finally, the normal wind load on element surfaces, determined by the product of the wind pressure and the exposed area, is modelled as a uniform force per unit length (in kN/m) acting on columns, whose value is calculated assuming the panels simply supported by the columns. The wind friction pressure is determined assuming the friction factor, c_f, equal to 0.02 (corresponding to "rough" surface, according to the Italian code).

Site	Wind zone	a_s (m)	v_b (m/s)	q_b (kN/m^2)	Terrain roughness	Exposure class	c_e	c_d
Milan	1	110	25.00	0.39		IV	1.63 1.84	
L'Aquila	3	714	31.32	0.61	B	IV	1.63 1.84	1
Naples	3	6	27.00	0.46		III	1.85 2.09	

Table 2: Wind load parameters.

Local meteorological climate conditions as well as the roof geometry, its thermal properties and exposure conditions influence the value of snow load on the roof. NTC 2008 [2] provides guidance for the determination of the snow load for structural design of buildings for sites at altitudes under 1500 m, accounting for all these aspects. The snow load on the roof, q_s, is derived multiplying the reference value of snow load on the ground, q_{sk}, by the three different factors provided in Table 3 (i.e., the snow load shape coefficient μ_i, the exposure coefficient C_E, the thermal coefficient C_t). The value of q_s for each site is given in the last column of Table 3.

Site	Climatic zone	a_s (m)	q_{sk} (kN/m^2)	μ_i	C_E	C_t	q_s (kN/m^2)
Milan	I - Mediterranean	110	1.50				1.20
L'Aquila	III	716	1.64	0.80	1.00	1.00	1.31
Naples	III	6	0.6				0.48

Table 3: Snow load on roof for different location sites.

The case studies are supposed to be equipped with overhead cranes. The machinery induces vertical and horizontal actions on the structure, with static and dynamic components. In addition to the self-weight, the structure is subjected to the vertical variable hoist load, horizontal variable forces caused by acceleration and deceleration of the crane due to its movement along the runway beams, horizontal forces caused by skewing of the crane also due to its movement along the runway beam. Each of those forces was modelled as a static equivalent action and evaluated according to the Italian code. Two positions of the crane, along the longitudinal direction of the building, are considered in order to obtain the worst load arrangements for ultimate and service conditions, and these correspond to the second and third portal frame alignment (see Figure 1), respectively.

Frame imperfections, including residual stresses and geometrical imperfections such as lack of verticality, lack of straightness, lack of flatness, lack of fit and eccentricities greater

than acceptable tolerances, are modelled by the simplified approach suggested by the Italian code: the effects of the global initial sway imperfection are replaced by systems of equivalent horizontal forces.

Earthquake motion at a point on the ground surface is represented by an elastic ground acceleration response spectrum $S_e(T)$. The horizontal seismic action is described by two orthogonal components (represented by the same response spectrum) and the vertical component response spectrum is considered as well. The seismic hazard parameters (a_g, F_0, T_c^*), reported in the Italian building code as a function of the geographical position and the reference return period, are shown in Table 4. The response spectra are derived assuming the topography condition T_1.

Site	Latitude	Longitude	Limit state	a_g (g)	F_o (-)	T_c^* (sec)
L'Aquila	13.396	42.356	DLS	0.104	2.330	0.280
			LLS	0.261	2.360	0.350
Naples	14.2600	40.850	DLS	0.059	2.330	0.310
			LLS	0.168	2.370	0.340
Milan	9.1900	45.4640	DLS	0.024	2.550	0.190
			LLS	0.050	2.660	0.280

Table 4: Hazard parameters.

Figure 4 shows the horizontal and vertical elastic response spectra for soil type A and C, for the life safety limit state (LLS).

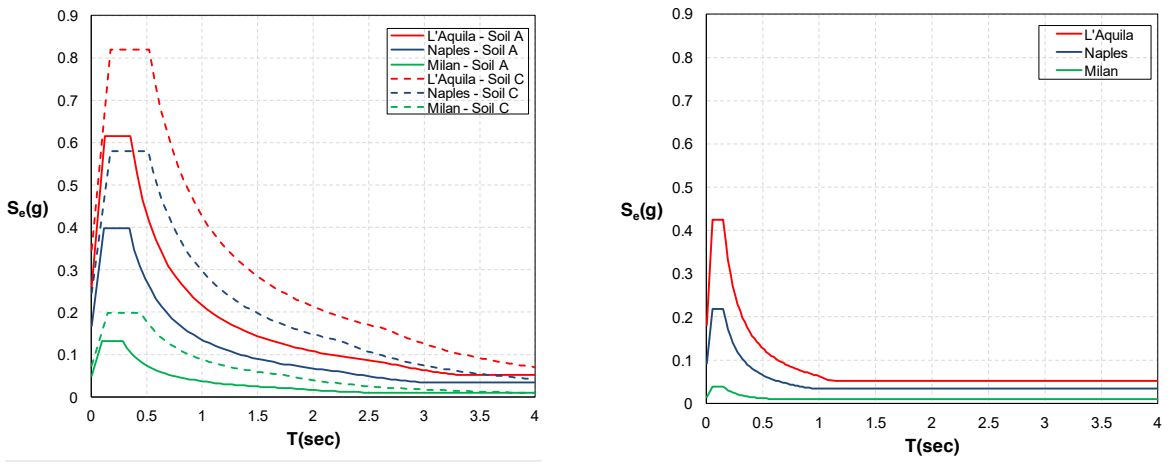

(a) (b)

Figure 4: Horizontal (a) and Vertical (b) elastic response spectra at LLS.

The case studies are designed by assuming a low-dissipative structural behaviour. Under this assumption, for both moment resisting frames and frames with concentric bracings, NTC 2008 [2] recommends a q-factor equal to 4, that is the factor used to reduce the elastic response spectra to obtain the design response spectra. The corresponding design response spectra obtained for Milan, L'Aquila and Naples, assuming soil types A and C, are shown in the following Figure 5.

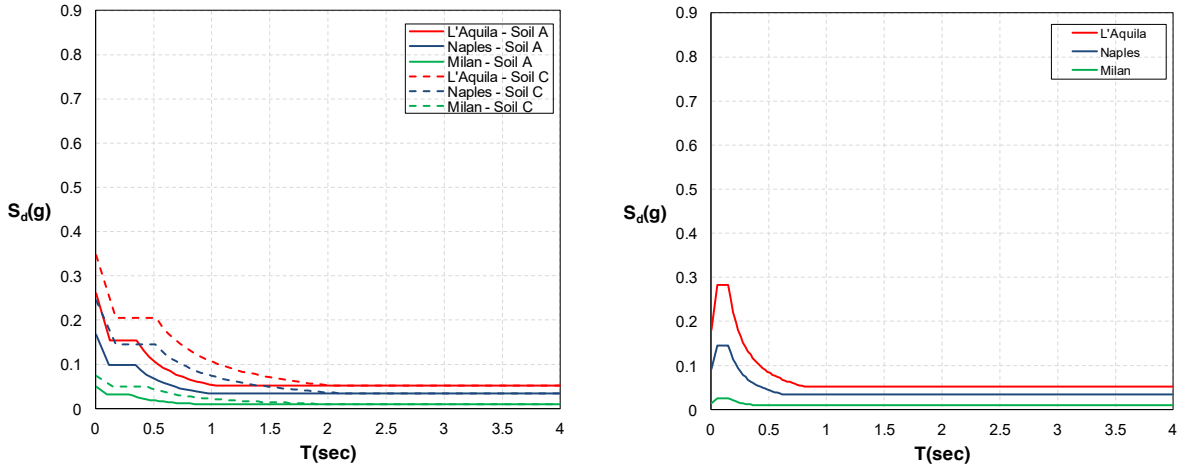

(a) (b)

Figure 5: Horizontal (a) and Vertical (b) design (reduced by q) response spectra al LLS.

Design combinations of the actions above described are made according to the Italian code considering the ultimate limit state (ULS) and the serviceability limit state (SLS), to ensure a safe and functional structure, respectively.

2.5 Global analysis for design

Maximum values of member forces and displacements are calculated by an elastic global analysis. Modal response spectrum analysis is performed to evaluate bending moments, axial forces and shear forces due to seismic actions. As recommended by NTC 2008 [2], seismic action effects are evaluated considering a number of vibration modes, such that the sum of the effective modal masses amounts to at least 85% of the total seismic mass. For the sake of clarity and due to space constraints, the first four mode shapes and the corresponding vibration periods are shown for the SSB_Lx20_Ly6_AQ case study only (Figure 6).

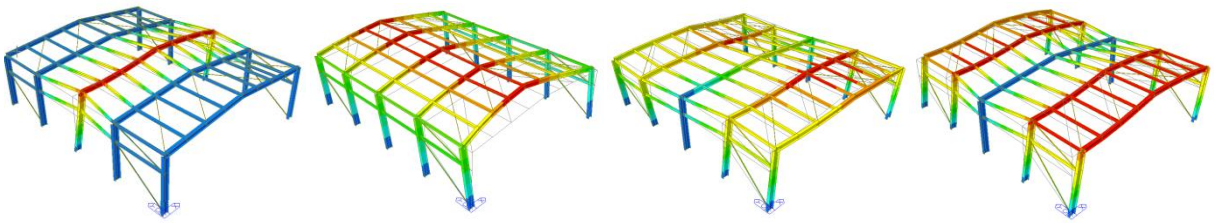

Mode=1; T=0.80 s Mode=2; T=0.50 s Mode=3; T=0.414 s Mode=4; T=0.412 s

Figure 6: First four modal shapes and natural vibration periods for SSB_Lx20_Ly6_AQ.

2.6 Structural design

Concerning ultimate limit state design, axial, bending and shear resistance and combined bending and axial force resistance of structural steel members are verified according to NTC 2008 [2]. When checking the rafter stability, the roof purlins are assumed to provide only lateral restraints, i.e. no additional torsional restraint is assumed at intermediate rafter locations. The column stability is checked assuming torsional restraints at the column bracket level. According to seismic design recommendations, the diagonal members of X-braced frames are designed such as their non-dimensional slenderness was in the range (1.3, 2). For single bay diagonal braces the non-dimensional slenderness is limited to 2.0. Serviceability limit state

verifications are performed to ensure that the deflections are acceptable at 'working loads'. Table 5 contains, for each case study, a list of cross-sections of all structural members. As shown, the 24 case studies resulted into only 9 different structural configurations.

Case Study	Column	Rafter	Vertical bracing X-braced – One braced		Long. beam	Purlins	Roof bracing
SSB_Lx20_Ly6_AQ_A SSB_Lx20_Ly6_AQ_C	HE 600 M	HE 500 A	RHS-CF-60x60x2	RHS-CF-90x90x2.6	IPE 270	HE 220 A	L20x3
SSB_Lx20_Ly8_AQ_A SSB_Lx20_Ly8_AQ_C	HE 600 M	HE 500 A	RHS-CF-70x70x2.6	RHS-CF-100x100x2.6	HE 300 B	HE 220 A	L20x3
SSB_Lx30_Ly6_AQ_A SSB_Lx30_Ly6_AQ_C	HE 900 M	HE 800 A	RHS-CF-80x80x2.6	RHS-CF-100x100x2.6	IPE 270	HE 220 A	L50x4
SSB_Lx30_Ly8_AQ_A SSB_Lx30_Ly8_AQ_C	HE 900 M	HE 800 A	RHS-CF-90x90x2.6	RHS-CF-120x120x3.2	HE 300 B	HE 220 A	L50x4
SSB_Lx20_Ly6_MI_A SSB_Lx20_Ly6_MI_C	HE 600 M	HE 450 A	RHS-CF-60x60x2	RHS-CF-90x90x2.6	IPE 270	HE 220 A	L20x3
SSB_Lx20_Ly8_MI_A SSB_Lx20_Ly8_MI_C	HE 600 M	HE 500 A	RHS-CF-70x70x2.6	RHS-CF-100x100x2.6	HE 300 B	HE 220 A	L20x3
SSB_Lx30_Ly6_MI_A SSB_Lx30_Ly6_MI_C	HE 900 M	HE 800 A	RHS-CF-80x80x2.6	RHS-CF-100x100x2.6	IPE 270	HE 220 A	L50x4
SSB_Lx30_Ly8_MI_A SSB_Lx30_Ly8_MI_C	HE 900 M	HE 800 A	RHS-CF-90x90x2.6	RHS-CF-120x120x3.2	HE 300 B	HE 220 A	L50x4
SSB_Lx20_Ly6_NA_A SSB_Lx20_Ly6_NA_C	HE 600 M	HE 450 A	RHS-CF-60x60x2	RHS-CF-90x90x2.6	IPE 270	HE 160 A	L20x3
SSB_Lx20_Ly8_NA_A SSB_Lx20_Ly8_NA_C	HE 600 M	HE 500 A	RHS-CF-70x70x2.6	RHS-CF-100x100x2.6	HE 300 B	HE 160 A	L20x3
SSB_Lx30_Ly6_NA_A SSB_Lx30_Ly6_NA_C	HE 900 M	HE 800 A	RHS-CF-80x80x2.6	RHS-CF-100x100x2.6	IPE 270	HE 160 A	L50x4
SSB_Lx30_Ly8_NA_A SSB_Lx30_Ly8_NA_C	HE 900 M	HE 800 A	RHS-CF-90x90x2.6	RHS-CF-120x120x3.2	HE 300 B	HE 160 A	L50x4

Table 5: Case study sections

In the X-direction, the design is governed by SLS deflection limits, in terms of horizontal deflection or difference of deflection between two consecutive portal frames. In the Y-direction, the cross section of the beams and diagonals is affected by the slenderness limits. Three different frames are derived: the beam-to-column combinations H 600 M - HE 500 A or H 600 M - HE 450 A satisfy deflection limits for SS_Lx20 configurations, whereas H 900 M - HE 800 A are suitable for all SSB_Lx30 geometries. Each transversal frame structure is connected in the Y-direction by two different longitudinal beams, depending on the Y-bay length: IPE 270 for L_y= 6 m and HEB 300 for L_y= 8 m. Four types of both X-braced diagonals and single diagonals are selected for the same number of diagonal lengths.

3 NONLINEAR FINITE ELEMENT MODELLING FOR SEISMIC ASSESSMENT

3.1 Model definition

The geometric and material nonlinear structural models for the seismic assessment of the considered case studies are developed within the OpenSees software [5]. In particular, all the structural elements are modelled using nonlinear force-based beam-column finite elements with fibre sections. The corotational approach is adopted in order to take into account the non-linear geometric effects due to both the large displacements and the local imperfections of the lateral bracing systems. Figure 7 shows a qualitative scheme of the finite element model.

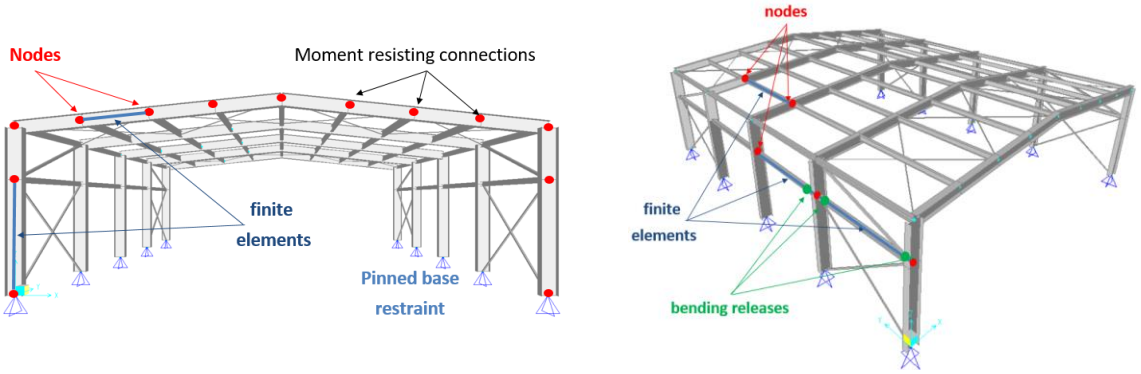

Figure 7: Finite element model, X (a) and Y (b) directions.

The elastic properties of each structural element are taken as follow: (i) elastic modulus E_s = 210 GPa; (ii) Poisson ratio ν = 0.3; (iii) shear modulus $G_s = E_s / 2(1+\nu)$ = 80.80 MPa; (iv) specific weight γ_s = 76.98 kN/m^3. The material nonlinear behaviour is modelled by assigning to each section's fibre the uniaxial Giuffre-Menegotto-Pinto steel material with isotropic strain hardening available in the OpenSees libraries. The linear elastic torsional stiffness ($J_t G_s$) is introduced by adding this contribution (in series) to that of the fibre section. The constitutive properties assumed for the stress-strain relationship are: (i) yielding strength f_y = 316.20 MPa [6]; (ii) post-elastic isotropic hardening ratio $E_p = 0.01E_s$; (iii) other constitutive law parameters governing the transition from the elastic to the inelastic branches assumed equal to default values as suggested in the OpenSees user manual [5]. The system's inner damping is accounted through the Rayleigh damping with ξ=5% on the first and third eigenvalues.

All columns are hinged at their bases. Loads are assigned as either point or distributed forces while the masses are lumped at the structural nodes according to their real spatial distribution and influence area.

3.2 Modelling of braces

Specific attention is given to the modelling of the braces constituting the seismic resisting elements along the Y-direction. There are two different configurations of lateral braces: a single brace configuration ad a X-configuration. The latter is made by two braces intersecting each other through a properly designed gusset plate connection; this connection needs one of the two braces to be cut (Figure 8).

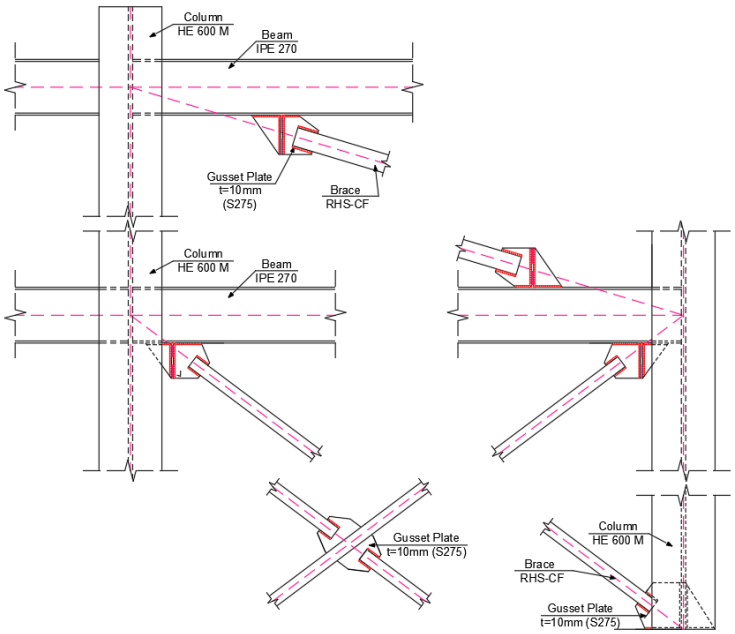

Figure 8: Lateral bracing system, details.

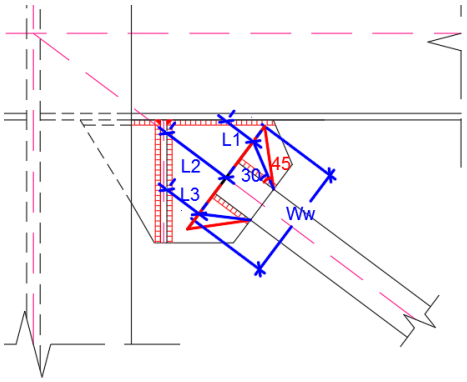

Figure 9: Geometrical quantities involved into the Gusset modelling.

The nonlinear spring is modelled in OpenSees through a zero-length element having the out-of-plane rotational degree of freedom represented by the same Giuffre-Menegotto-Pinto steel material. In order to simulate the buckling of the lateral braces during the compression phases, each brace has been discretized into a proper number of nonlinear (with distributed plasticity) sub-elements and a sinusoidal curvature is assigned by modifying parametrically the coordinates of the nodes of the intermediate sub-elements (Figures 10 and 11). This initial curvature, representing the local imperfection of the diagonal brace, has the role of triggering the buckling by furnishing a preferential buckling shape to the element. The value of the initial imperfection is chosen in such a way to provide a buckling axial force consistent with the ultimate value $N_{b,Rd}$ provided by Equation (2):

$$N_{b,Rd} = \frac{\chi \cdot A \cdot f_y}{\gamma_{M1}} \tag{2}$$

with $\gamma_{M1} = 1$, A = cross section area, f_y = nominal yielding stress and χ = the buckling reduction factor depending on the profile type and the slenderness of the element. For this purpose,

each single brace is extracted from the whole structure and modelled separately, according to its actual section and configuration (i.e., length and gusset connections), and then is subjected to several nonlinear static analyses (controlled by displacements) repeated with a sequence of different values of the initial imperfection. This procedure converges once the maximum axial force reached during the analysis matches the $N_{b,Rd}$ provided by the code formula.

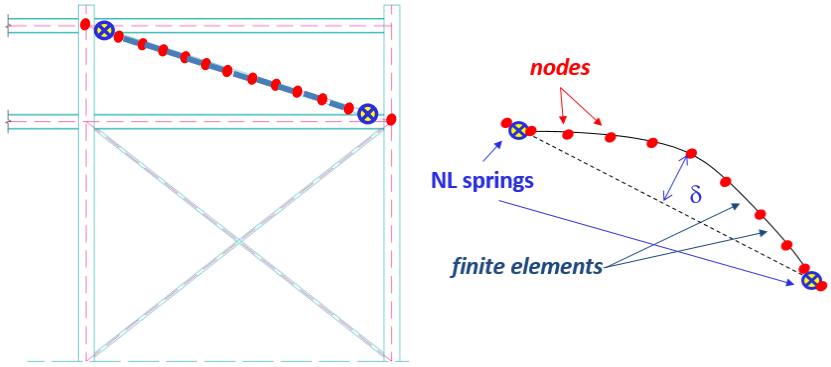

Figure 10: Single brace (a) NL springs and sub-elements and (b) initial imperfections.

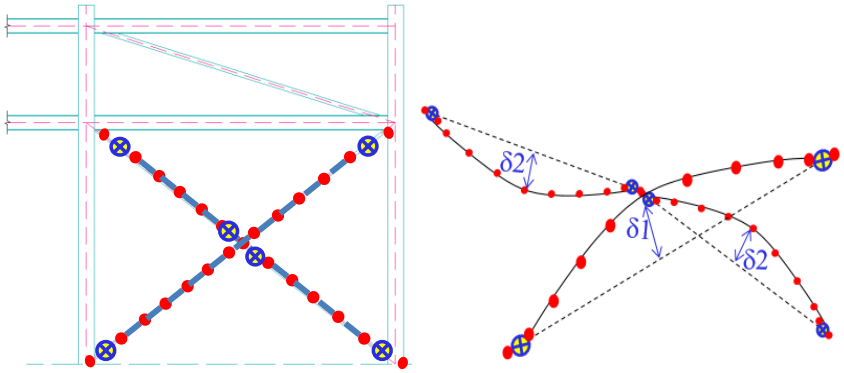

Figure 11: X brace (a) NL springs and sub-elements and (b) initial imperfections.

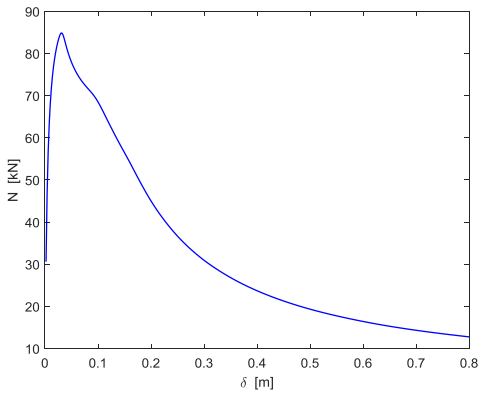

Figure 12: N-δ curve for single braces ($N_{b,Rd}$ = 85 KN).

Figure 12 shows, as an example, the axial force versus lateral displacement (N-δ, with δ observed at the middle of the element) curve, which is obtained by assigning an imperfec-

tion equal to $L_{eff}/1000$ to the single brace and by performing a nonlinear static analysis controlled by displacements (the sign of the displacements in the chart is positive for brace shortening). The value of $N_{b,Rd}$ provided by the code for this element with its geometry and slenderness is $N_{b,Rd}$ = 85 kN, and the maximum value reached by the axial force during the analysis is exactly 85 kN, meaning that the imperfection $L_{eff}/1000$ is consistent with the code provisions.

The modelling technique presented allows accounting for the complex cyclic behaviour of the lateral braces. Figure 13 shows, as an example, the force-displacement cyclic response of a lateral brace under a displacement-controlled test and the moment-rotation cyclic response of the gusset plate, both simulated with OpenSees.

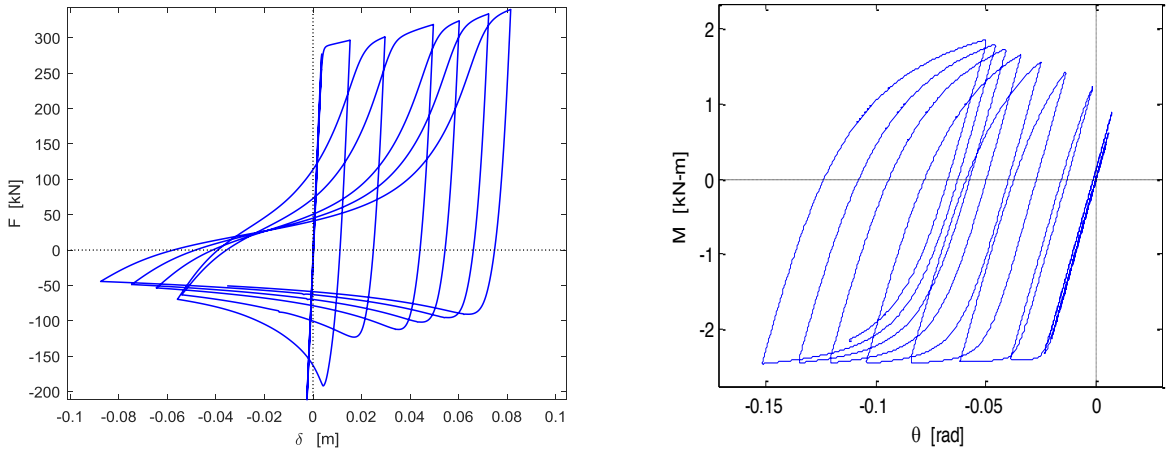

(a) (b)

Figure 13: (a) F-δ curve of a single brace and (b) gusset plate rotational cyclic behaviour.

3.3 Push-over analysis

A preliminary investigation of the nonlinear lateral behaviour of the structure is carried out by means of nonlinear static analysis (push-over). A set of forces with unit values is applied to the structural nodes at the top of the columns and separately along the X and Y directions. Figure 14 shows the X and Y control nodes monitored during the analysis.

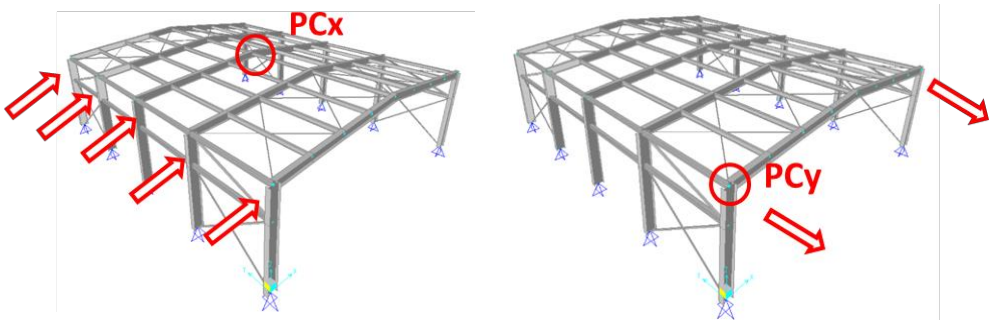

(a) (b)

Figure 14: Push-over lateral loads for (a) X and (b) Y directions.

Push-over analyses are carried out by performing a preliminary analysis for gravity loads and by starting the lateral loads analysis from the last step of the previous analysis. Gravity

loads analysis is performed with a load-control integrator using the Newton algorithm (tangent stiffness updated at each iteration) in such a way that the gravity is applied with 10 steps of 0.1g. The lateral loads analysis is carried out using a displacement-control integrator and the secant Newton line search algorithm. The step amplitude is equal to 1 mm while the target maximum displacement is generally assumed large enough for a complete development of the post-elastic behaviour.

The structure shows different responses in X and Y directions as illustrated by the push-over curves in Figure 15. The maximum displacement reached along the X direction at the control point is 0.5 m and no softening is observed. Quite different is the longitudinal response in which both the second order effects and the compressed braces buckling leads to a post-elastic behaviour characterized by an initial branch with negative stiffness (softening) followed by a gradual stiffness recover due to the steel hardening, whose contribution is large enough to compensate and even overtake the second order effects.

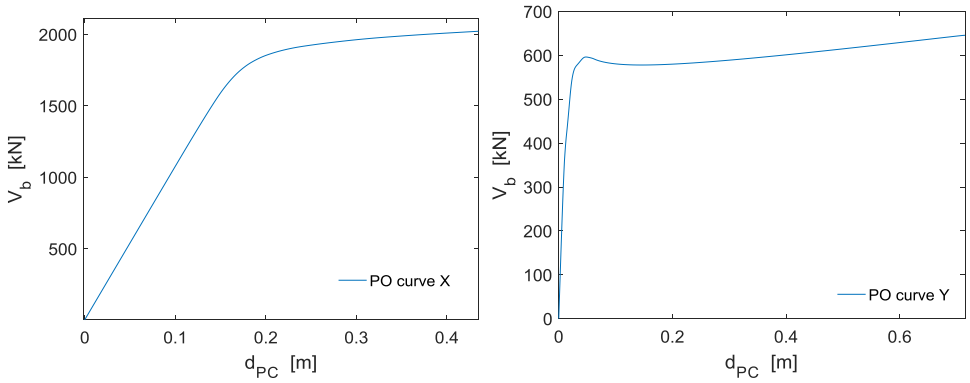

Figure 15: Push-over capacity curves for (a) X and (b) Y directions.

Figure 16 reports the lateral deformation of the system at an intermediate step of analysis in order to show qualitatively the buckling phenomenon experienced by the compressed braces. The most pronounced second order effect is observed on the central portal frame, which, around the last steps of analysis shows larger displacements than the other portals, despite the entity of the lateral loads is the same as for the others. This phenomenon finds an explanation into the lacking of a roof-bracing system around that portal, and the longitudinal (pinned) beams do not contribute to retain the portal but, on the contrary, they show an axial elongation (i.e., they work as a chain system) due to the second order effects. In Figure 17 the transversal deformation is shown by both a front and top view.

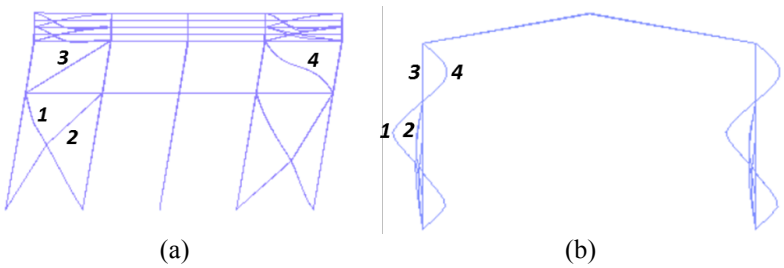

Figure 16: System deformation (Push-over Y) and braces numbering, (a) lateral and (b) frontal view.

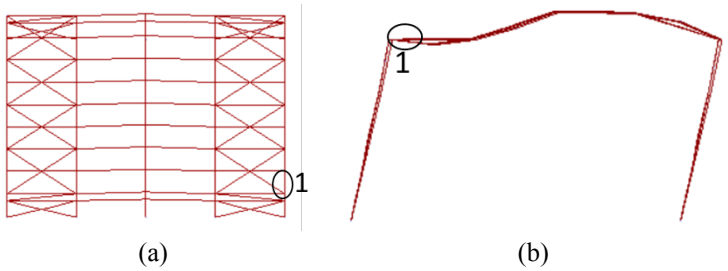

(a) (b)

Figure 17: System deformation (Push-over X) and beam numbering, (a) top and (b) frontal view.

3.4 Multi-record incremental dynamic analysis

Multi-record incremental dynamic analysis are carried out for 10 intensity levels by using a set of 20 pairs of accelerograms (each seismic event is made of two horizontal accelerograms, neglecting the vertical seismic component) in order to simulate the record-to-record variability. The spectral pseudo-acceleration at the fundamental period of the system is chosen as intensity measure (IM). This means that each one of the 20 accelerograms is scaled at each IM level in order to provide the same spectral pseudo acceleration ordinate $S_a(T_1)$ at the system period T_1. In the considered case studies two periods are adopted, i.e. 0.5 s and 1.0 s for the portal frame lengths equal to 20 m and 30 m, respectively. More details on record selection and scaling are found in the relevant companion paper.

Each time-history analysis has a starting point coincident with the last step of a nonlinear static analysis for gravity loads, as done for the push-over analysis. The two accelerograms in the X and Y directions are applied simultaneously at the base of the structures and the solver adopted consists of a standard Newmark integration with a secant Newton line search algorithm controlling the iterations for the convergence of the solution. The time-steps of the analysis are chosen adaptively by the OpenSees solver within a range between 0.0005 s and the time-step used for sampling the seismic records.

Structural collapse is identified in the post-processing of results. Specifically, different criteria are used for the two directions, i.e., transversal moment-resisting frames and longitudinal concentrically braced frames. For the moment-resisting frame, the collapse criterion is based on a limit value of the inter-storey drift according to the suggestions of FEMA-350 [7] (assumed value 0.10) that conservatively and conventionally account for the global response of the building and the local behaviour of beam-column connections. Regarding the collapse criterion for the concentrically braced frames, the limit is assigned to the maximum strain range in the braces, according to the indications in Hsiao et al. [8][9] and Tirca et al. [10], having assumed as limit value of 0.0049 following the experimental tests by Tremblay et al. [11].

A selection of the results obtained though the adoption of the above collapse criteria provided the results summarized in Figure 18. It is observed that: (i) the trend of the EDP considered in the collapse criterion is different for the moment-resisting frame and the concentrically braced frame, i.e. the former has a more progressive increment with the IM value, while the latter has a more sudden increment, as expected given the effect of brace buckling on the seismic response; (ii) collapse is attained only in the L'Aquila site for IM values larger than those considered in the limit states considered in the design; (iii) collapse is not attained by a good margin for the Naples site for any IM (except for isolated cases with IM = 10) and by a very large margin for the Milan site for any IM.

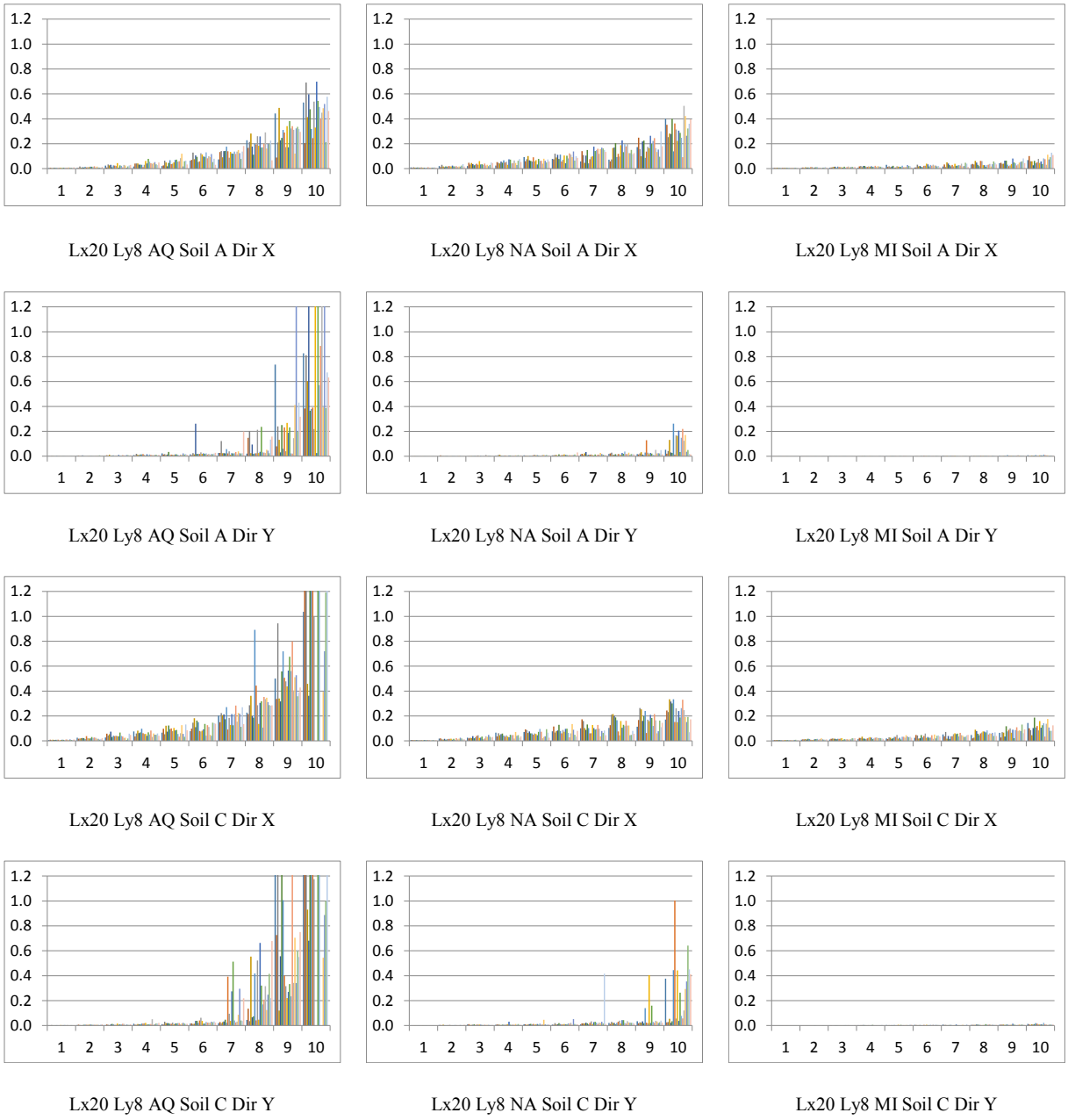

Figure 18: Ratio between EDP and limit value of EDP at collapse (ordinates) as a function of the 10 IM considered (abscissa) for each of the 20 accelerograms.

4 CONCLUSIONS

This paper presents the results of an ongoing project on computing the implicit risk of seismic collapse of buildings designed according to the current Italian design code NTC2008. The paper focuses on a set of non-residential single-storey steel buildings in three sites of increasing seismic hazard. The results from multiple-stripe analyses (20 nonlinear time history analysis for 10 intensity levels) show that the only buildings showing collapse are those in L'Aquila (the site with the highest hazard level) and only for the last stripes corresponding to extremely long return periods.

ACKNOWLEDGEMENTS

The authors would like to acknowledge the financial support of the Italian Civil Protection Department, ReLUIS project 2014-2018 (http://www.reluis.it/).

REFERENCES

[1] I. Iervolino, A. Spillatura, P. Bazzurro, RINTC Project - Assessing the (implicit) seismic risk of code-conforming structures in Italy. COMPDYN 2017 - 6th ECCOMAS Thematic Conference on Computational Methods in Structural Dynamics and Earthquake Engineering M. Papadrakakis, M. Fragiadakis (eds.) Rhodes Island, Greece, 15–17 June 2017.

[2] NTC 2008, Norme Tecniche per le Costruzioni, Decreto Ministeriale del 14 gennaio 2008, in Italian (Italian Building Code, 2008).

[3] Midas GEN v2.1 2016, Integrated Solution System for Building and General Structures. Midas Information Technology Co. Ltd.

[4] CEN. Eurocode 3: Design of Steel Structures, Part 1-1, General Rules and Rules for Buildings. CEN, Brussels: European Committee for Standardization, 2005.

[5] Mazzoni, S., McKenna, F., Scott, M.H., Fenves, G.L. et al., "Opensees Command Language Manual", PEER Website, July 2007.

[6] L.S. Da Silva, C. Rebelo, D. Nethercot, L. Marques, R. Simões, P.V. Real, Statistical evaluation of the lateral–torsional buckling resistance of steel I-beams, Part 2: Variability of steel properties. *Journal of Constructional Steel Research*, **65**(4), 832-849, 2009.

[7] Federal Emergency Management Agency, Recommended Seismic Design Criteria for New Steel Moment-Frame Buildings, FEMA 350, June 2000.

[8] P.C. Hsiao, D.E. Lehman, C.W. Roeder, Improved analytical model for special concentrically braced frames. *Journal of Constructional Steel Research*, **73**, 80-94, 2012.

[9] P.C. Hsiao, D.E. Lehman, C.W. Roeder, Evaluation of the response modification coefficient and collapse potential of special concentrically braced frames. *Earthquake Engineering & Structural Dynamics*, **42**(10), 1547-1564, 2013.

[10] L. Tirca, L. Chen, R. Tremblay, Assessing collapse safety of CBF buildings subjected to crustal and subduction earthquakes, *Journal of Constructional Steel Research* **115**(1):47-61, 2015.

[11] R. Tremblay, M.H. Archambault, A. Filiatrault, Seismic response of concentrically braced steel frames made with rectangular hollow bracing members. *Journal of Structural Engineering*, **129**(12):1626-1636, 2003.